

Deep Image Compression using Decoder Side Information

Sharon Ayzik
Tel-Aviv University
ayziksha@mail.tau.ac.il

Shai Avidan
Tel-Aviv University
avidan@eng.tau.ac.il

Abstract

We present a Deep Image Compression neural network that relies on side information, which is only available to the decoder. We base our algorithm on the assumption that the image available to the encoder and the image available to the decoder are correlated, and we let the network learn these correlations in the training phase.

Then, at run time, the encoder side encodes the input image without knowing anything about the decoder side image and sends it to the decoder. The decoder then uses the encoded input image and the side information image to reconstruct the original image.

This problem is known as Distributed Source Coding in Information Theory, and we discuss several use cases for this technology. We compare our algorithm to several image compression algorithms and show that adding decoder-only side information does indeed improve results. Our code is publicly available ¹.

1. Introduction

Deep Image Compression uses Deep Neural Networks (DNN) for image compression. Instead of relying on hand-crafted representations to capture natural image statistics, DNN methods learn this representation directly from the data. Recent results show that indeed they perform better than traditional methods.

Ultimately, there is a limit to the compression rate of all methods, that is governed by the rate-distortion curve. This curve determines, for any given rate, what is the minimal amount of distortion that we must pay. We can break this barrier by introducing side information that can assist the network in compressing the target image even further.

Figure 1 gives an example of results obtained by our system. The top row shows the results of a state-of-the-art deep image compression algorithm. The bottom image shows the results of our method that relies on side information. As can be seen, our method does a better job of restoring the details.

¹<https://github.com/ayziksha/DSIN>

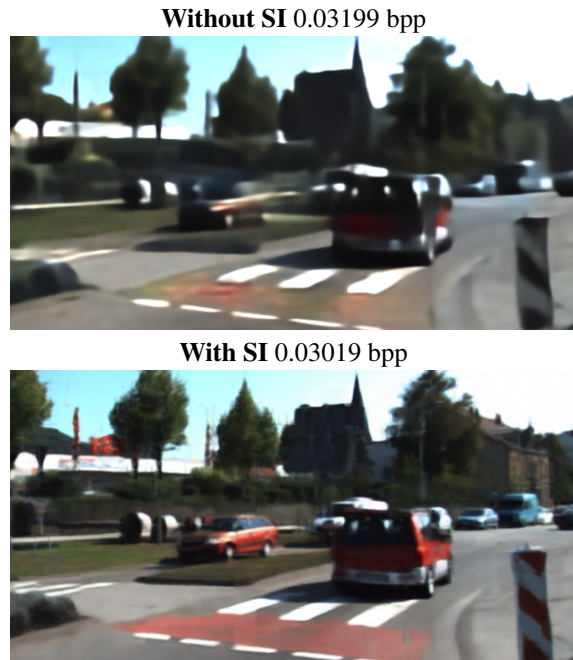


Figure 1. Reconstruction for very low bit per pixel (bpp) using side information (SI) can restore fine details. Note the small red car, the crosswalk, the building to the back right side with the blue vehicle, and even the trees textures.

One can catalogue image compression schemes into three classes (see Figure 2). The first (top row) is a standard image compression scheme. Such a network makes no use of side information, and the trade-off is governed by the rate-distortion curve of the image.

Deep Video Compression (second row in Figure 2) goes one step further and in addition to natural image statistics, also relies on previous frames as side information that is available to both the encoder and the decoder. The availability of this side information improves the compression ratio of video compared to images. The limit of this scheme is bounded by the conditional probability of the current frame given previous frames. This works well when the two frames are correlated, as is often the case in video.

We consider a particular scenario in which the side information is only available to the decoder side. This scenario is a special case of the Distributed Source Coding (DSC) problem in the field of Information Theory (third row of Figure 2). It turns out that even in this case, the compression scheme can benefit from side information. That is, DSC can, in theory, achieve the same compression ratios as deep video compression, which is much better than single image compression. But when does this scenario occur in practice?

It turns out that this DSC scenario occurs quite frequently, and here are a couple of examples. Consider the case of a camera array. For simplicity, we focus on a stereo camera, which is the simplest of camera arrays. The left and right cameras of the stereo pair are each equipped with a micro-controller that captures the image from the camera, compresses it, and sends it to the host computer. Since both cameras capture the same scene at the same time, their content is highly correlated with each other. But since the left and right cameras do not communicate, they only communicate with the host computer and can not use the fact that they capture highly correlated images to improve the compression ratio. This puts a heavy burden on the host computer, which must capture two images in the case of stereo camera and many more in the case of a camera array.

Now suppose that the left camera transmitted its image to the host computer and the right camera as well. Then the right camera can encode its image conditioned on the left image and transmit fewer bits to the host computer. This reduces the burden on the host computer at the cost of sending the left image to the right camera. Distributed Source Coding theory tells us that we do not have to transmit the image from the left camera to the right camera at all, and still achieve the same compression ratio. When considering a camera array with multiple cameras, the savings can be substantial.

Camera arrays are assumed to be calibrated and synchronized, but we can take a much more general approach. For example, a group of people taking pictures of some event is a common occurrence nowadays. We can treat that as a distributed, uncalibrated, and unsynchronized camera array. Instead of each person uploading his images to the cloud, we can pick, at random, a reference person to upload his images to the cloud and let the rest of the people upload their images conditioned on the reference images. Taking this idea one step further, assume that a single person takes a picture and uploads it to the cloud. If we further assume that the position and orientation of the camera are known, then we can use previous images that were captured at this location in the past as our side information.

Our approach is using recent advances in deep image compression, where we add side information to the decoder side. During training, we provide the network with pairs of

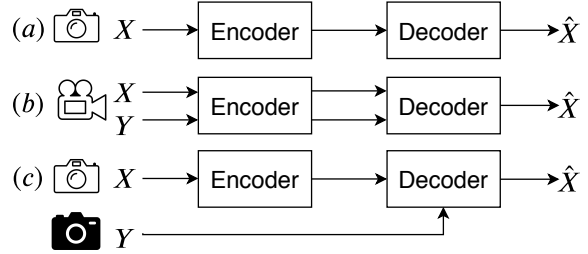


Figure 2. Different compression schemes. (a) Single image encoding-decoding. (b) Video coding: joint encoding-decoding. The successive frame Y is used as side information. (c) Distributed source coding - image X is encoded and then decoded using correlated side information image Y .

real-world, correlated images. The network learns to compress the input image, and then add the side information image to help restore the original image. At inference time, the encoder is used for compressing the image before transmitting it. The rest of the network, which lies at the receiver side, is used by the decoder to decode the original image, using the compressed image and the side information image.

We evaluate our system on two versions of the KITTI dataset that are designed to simulate the scenarios described earlier. In the first, we use the KITTI Stereo dataset to simulate the scenario of a camera array (in this case, a stereo camera). In the second case, we use pairs of images from the KITTI Stereo dataset that are taken several frames apart. This case is designed to simulate the scenario where an image is uploaded to the cloud, and some other image, from the same location, is used as side information.

2. Related work

Deep compression: Using DNN in many applications has gained much popularity in recent years, the same goes for the task of image compression. Common usage of DNN for the task of compression are RNNs [25, 26] and auto-encoders [33, 4, 17]. The networks are usually designed in an end-to-end manner, aiming to minimize the final loss on the decompressed image.

Toderici *et al.* [25, 26] used progressive image compression techniques and tested various types of recurrent neural networks to create a hybrid network that extracts a binary representation code using an entropy coder. Ballé *et al.* [4] used quantization rather than binarization. Theis *et al.* [24] use a simple approximation to replace the rounding-based quantization, in addition to bounding the discrete entropy loss. And Mentzer *et al.* [17] use an auto-encoder and a context model that learns to assess the distribution of the bit-stream in addition to an importance map to improve performance.

Recent work by Agustsson *et al.* [3] suggests using GAN based architecture to break the rate-distortion bounds. They encode the image with fewer bits than what is dictated by the rate-distortion curve. Then they use a GAN, on the decoder side, to synthesize a similar image that is visually pleasant.

Building on the success of Deep image compression schemes, we witnessed the emergence of Deep video compression schemes. Early work replaced various steps in the video compression scheme with a DNN counterpart. For example, Lu *et al.* [16] use a deep network to remove compression artifacts in the post-processing step. Tsai *et al.* [27] use an auto-encoder to compress the residuals of an H.264 encoder. Wu *et al.* [31] treat video compression as a repeated image interpolation and build a full network for that. Recently, Lu *et al.* [16] proposed a network that replaces all the components of a video encoder with a single end-to-end architecture.

Distributed Source Coding: Distributed Source Coding (DSC) started with the groundbreaking result of Slepian-Wolf [22, 10] who proved that it is possible to encode a source X given a correlated source Y even if Y is only available to the decoder side. This result applied to the lossless case and was later extended by Wyner-Ziv [32] to the lossy case by first quantizing the continuous signal and then applying the Slepian-Wolf theorem.

Although the theory of DSC dates back to the '70s, it was only 30 years later that its first practical implementation was presented. One of the most important works was done by Pradhan and Ramchandran - Distributed Source Coding Using Syndromes (DISCUS) [20]. They presented a practical framework for the asymmetric case of source coding with side information at the decoder, based on sending the syndrome of the code-word coset for statistically dependent binary and Gaussian sources.

Much of the work on DSC was in the context of lightweight video compression. That is, instead of running a standard video compression scheme (i.e., MPEG) that requires motion estimation on the encoder side [15], DSC offers the possibility of shifting the computational load from the encoder to the decoder. This scheme is useful, for example, in the case of a smartphone that needs to send a video to the cloud. For example, Girod *et al.* [2, 1, 12] focused on Distributed Video Coding (DVC). The video sequence was split to odd and even frames, the odd frames were used as side information at the decoder while Wyner-Ziv coding was applied to the even frames.

In [28, 8] the authors apply DSC to stereo images, in which one encoded image is decoded with reference to side information derived from disparity-compensated versions of the other image and in the latter an additional use of gray code is done.

3. Deep Distributed Source Coding

Toy Example: To gain some intuition into the DSC problem, consider the following toy example. Suppose X and Y are two 8-bit gray-scale images that are known to be aligned such that pixel $X(i)$ corresponds to pixel $Y(i)$. Assume image X is available to the encoder on the smartphone, and image Y is available to the decoder in the cloud. Transmitting X to the cloud requires 8-bits per pixel. But what if the corresponding pixels, $X(i), Y(i)$ are correlated? For example, they satisfy the following correlation: $|X(i) - Y(i)| \leq 3$. How can we take advantage of this correlation? A moment of thought shows that given $Y(i)$, $X(i)$ can only take seven different values, so we should hope to encode $X(i)$ using only 3 bits and not 8.

How can we do this in practice? Here is a numerical example. Let $X(i) = 110$ and $Y(i) = 113$. Consider the following DSC scheme: the encoder computes $6 = \text{mod}(X(i), 8)$ and sends the number 6 to the cloud using only 3 bits. The modulo operation created a *coset* $\{6, 14, 22, \dots, 102, 110, 118, \dots, 254\}$ of pixel values. Every element x of this coset satisfy the constraint that $\text{mod}(x, 8) = 6$. And, by construction, the minimal distance between any pair of elements in the coset is at least 8. Given these facts, the decoder knows that the unknown $X(i)$ must be one of the elements in the coset. It also knows that $|X(i) - Y(i)| \leq 3$. Given that $Y(i) = 113$, the decoder can deduce that $X(i)$ must be 110. We have encoded X using only 3 bits per pixel, instead of 8. Observe that the encoder did not know the value of pixel $Y(i)$ that is only available to the decoder. The prior information on the correlation between the two images is sufficient.

DSC for images: DSC was applied to video compression, where successive frames are almost aligned. This near alignment was enough to assume that patches in successive frames that are in the same location in the image plane are correlated. Moving to general settings, as the ones discussed in this paper, presents a new challenge. We can no longer assume that the two images are aligned, nor that the layout of the images is similar. For example, we would like two images containing a house next to a tree to be correlated even if the tree is to the right of the house in one image, and is to the left in the other.

One way to address this challenge is to break the two images into patches and use patches to measure the correlation between the images. But this raises a new problem- instead of having one (image) X and one (image) Y , we now have multiple (patches) X and multiple (patches) Y . Now, if we use the coset trick, then we don't know which patch in Y to use, because the images are not aligned.

We have conflicting demands. On the one hand, we need to transmit sufficient information about a patch in X , to al-

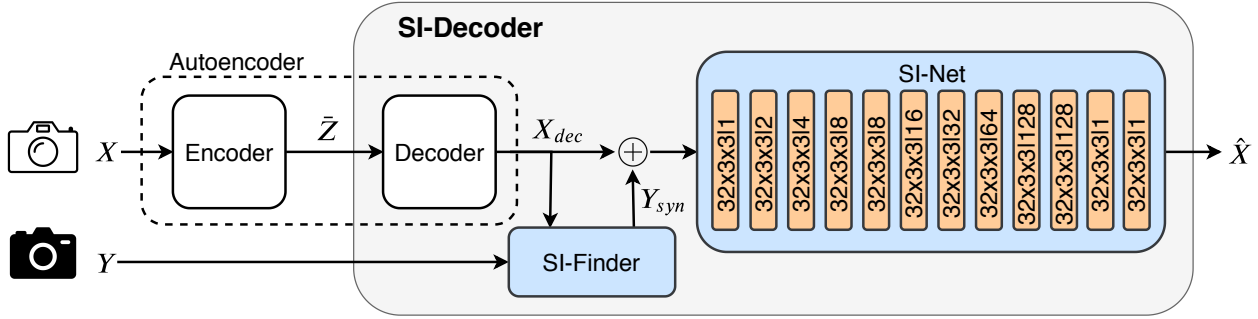


Figure 3. Our network’s architecture. The image X is encoded to \bar{Z} and decoded to the image X_{dec} using the auto-encoder model based on [17]. X_{dec} is used to create Y_{syn} using the SI-Finder block that finds for each patch in X_{dec} , the closest patch in Y . X_{dec} and Y_{syn} are concatenated (marked as \oplus) and forwarded to the SI-Net block that outputs the final reconstruction - \hat{X} . The SI-Net block is based on [9] and uses convolution layers with increasing dilation rates that approximate increasing the convolutions receptive field. $C \times K \times K$ notation in the SI-Net block refers to $K \times K$ convolutions with C filters. The number following the pipe indicates the rate of kernel dilation.

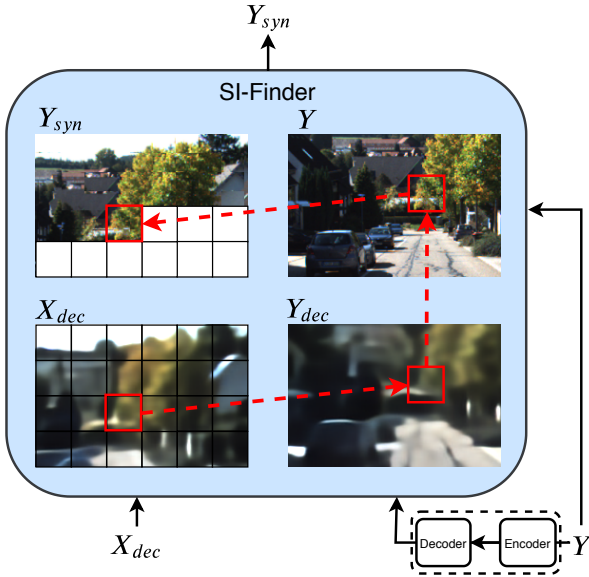


Figure 4. SI-Finder block illustration. Each non-overlapping patch in image X_{dec} is compared to all possible patches in Y_{dec} . The location of the maximum correlation patch in Y_{dec} is chosen and the patch is taken from Y image in the same location. Finally, the patch is placed in Y_{syn} in the corresponding X_{dec} patch location.

low the decoder to pick the correlated patch in Y . On the other hand, we only wish to transmit a code for the coset and let the decoder use that, together with the corresponding patch in Y , to recover the correct patch in X . We solve the DSC problem for images using a Deep Neural Network.

3.1. Architecture

The overall architecture of the network is given in Figure 3. The encoder has access to the input image X , and

the decoder has access to a correlated image Y . Our architecture consists of two sub-networks, the first is an auto-encoder designed for image compression and based on the model of Mentzer *et al.* [17]. It takes the input image X and produces the decoded image X_{dec} . The second network takes the decoded image X_{dec} along with image Y and use it to construct a synthetic side information image Y_{syn} . The decoded image X_{dec} and synthetic side information Y_{syn} are then concatenated and used to produce the final output image \hat{X} . The entire network, consisting of both sub-networks, is trained jointly. Then, at inference time, the encoder uses the encoder part of the auto-encoder sub-network, while the decoder uses the rest of the network.

It should be noted that the quantized latent vector \bar{Z} of our auto-encoder network is not designed to reconstruct the original image X , nor is it designed to create a coset from which the decoder can recover the correct X . Its goal is to provide sufficient information to construct a good synthetic image Y that, together with the decoded image X_{dec} , can be used to recover the final result \hat{X} . This means it should reconstruct an image X_{dec} that has sufficient details to search for good patches in Y that are as correlated, as much as possible, with their corresponding patches in X .

Formally, image compression algorithms encode an input image X to some quantized latent representation \bar{Z} from which they can decode a reconstructed image X_{dec} . The goal of the compression is to minimize a distortion function. The trade-off between compression rate and distortion is defined by:

$$d(X, \hat{X}) + \beta H(\bar{Z}) \quad (1)$$

where $H(\bar{Z})$ is the entropy of \bar{Z} (i.e., the bit cost of encoding \bar{Z}), $d(X, \hat{X})$ is the distortion function and β is a scalar that determines the trade-off between the two.

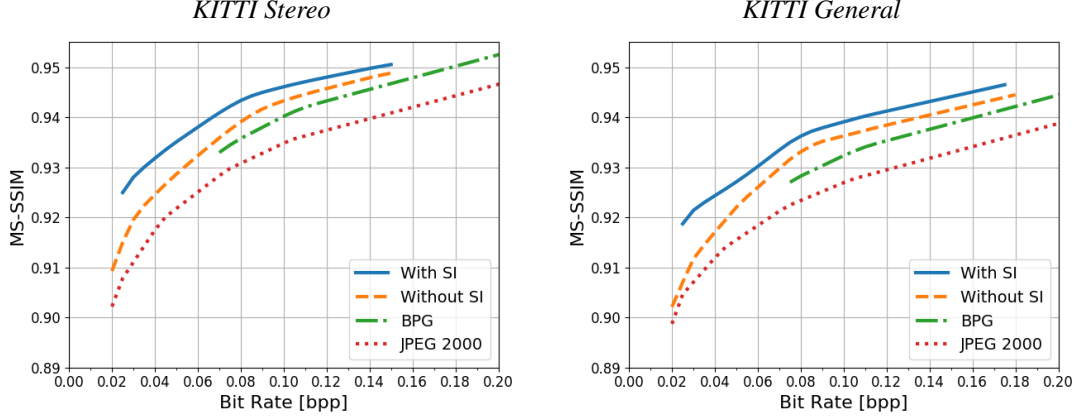


Figure 5. Rate-Distortion curve - MS-SSIM as a function of bit rate on both datasets. We outperform the baseline model (without side information) as well as BPG and JPEG 2000.



Figure 6. Top to bottom: Examples from *KITTI Stereo* and *KITTI General* compressed using the different codecs.

3.2. Using Side Information

We wish to minimize (1) given a correlated image Y that is only available to the decoder. To do that, we wish to create an image Y_{syn} from Y that is aligned with X . Let f encode the offset of every patch in X_{dec} to its corresponding patch in Y_{dec} , where Y_{dec} is the result of passing Y through the auto-encoder:

$$f(i) = \underset{j}{\operatorname{argmax}} \operatorname{corr}(\pi(X_{dec}(i)), \pi(Y_{dec}(j))) \quad (2)$$

where $\operatorname{corr}(\cdot)$ is a correlation metric, $\pi(X_{dec}(i))$ is the patch around pixel $X_{dec}(i)$. Then the synthetic image Y_{syn} is given by:

$$Y_{syn}(i) = Y(f(i)) \quad (3)$$

That is, Y_{syn} is a reconstruction of X from Y . We perform this reconstruction step in the SI-Finder block, that is

illustrated in Figure 4. It receives the images X_{dec} and Y , creates Y_{dec} by passing Y through the auto-encoder, and compares each non-overlapping patch in X_{dec} to all possible patches in Y_{dec} . This creates a (sparse) function f that is then used to create Y_{syn} from Y .

Eventually we feed X_{dec} and Y_{syn} to the SI-Net block and let it try to reconstruct X . Since we use concatenation of X_{dec} to the side information image Y_{syn} during training, we must maintain a reconstruction loss over X_{dec} . Therefore, the total rate-distortion trade-off from (1) is set to be:

$$(1 - \alpha) \cdot d(X, X_{dec}) + \alpha d(X, \hat{X}) + \beta H(\bar{Z}) \quad (4)$$

where α denotes the weight for the final system's output \hat{X} , and the total distortion weight sums to 1 in order to maintain the balance between the distortion and the rate.

4. Experiments

We discuss the datasets we use and the training procedure in section 4.1, and then present the results of our experiments in section 4.2.

4.1. Implementation details

Datasets: We constructed our datasets from the KITTI 2012 [11] and KITTI 2015 [18, 19] datasets. Our datasets are designed to approximate the two settings discussed in section 1.

The first termed *KITTI Stereo*, consists of 1578 stereo pairs taken from the calibrated stereo camera in the KITTI stereo datasets. It is designed to illustrate the camera array use case.

The second termed *KITTI General*, consists of 789 scenes with 21 images per scene. We constructed the dataset from pairs of images where one image is taken from the left camera of the stereo rig, and the second image is taken from the right camera, 1 to 3 frames down the road with a maximum distance of ~ 9 meters. This dataset is designed to simulate the case of uploading an image (e.g., the left image) to the cloud where a correlated image (the right image several frames apart) is already stored there and retrieved, for example, using GPS coordinates.

Training: We implemented our model in *TensorFlow*. For each dataset and bit rate in the range of 0.02 to 0.2 bits per pixel (bpp), we trained the baseline model (i.e., auto-encoder only) according to the training details in [17], using L_1 reconstruction loss. Then we trained the full model with image size of 320×960 for 300K iterations (which took around 24h per model on a single GPU), using the pre-trained auto-encoder weights as initialization and L_1 loss on both the auto-encoder and the final output - \hat{X} with the trade-off weight $\alpha = 0.7$ from (4). We used Adam [14] optimizer with an initial learning rate of $1 \cdot 10^{-4}$ and a batch size of 1 (i.e., each iteration included a pair of images X, Y). When training the full model, the original image size was used to enable the SI-Finder module full freedom of choice for locating the best patch possible for any given patch of X_{dec} . As for the SI-Finder block, we used a patch size of 20×24 , and the similarity measure between patches was chosen to be the Pearson correlation on images transformed with RGB color space according to [7]. We tested our models on 790 images for *KITTI Stereo* and 556 for *KITTI General* with size of 320×1224 .

4.2. Results

We evaluated our results by an averaged rate-distortion curve using MS-SSIM [30]. We compared our baseline model without side information (i.e., auto-encoder only) to the model trained with side information. In addition,

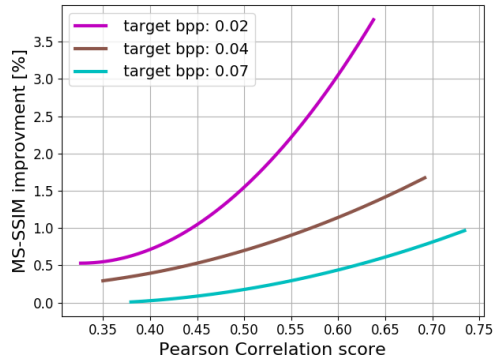


Figure 7. Correlation vs. Side-Information contribution on the *KITTI General* dataset. The x -axis is the Pearson correlation between X and Y_{syn} . The y -axis is the ratio of the MS-SSIM score with and without side information. Each nonlinear curve represents a different model trained to a different target bpp. As can be seen, higher correlation leads to better reconstruction results.

we compare ourselves to JPEG 2000 [23] and to BPG [6] (HEVC based codec that surpassed all other codecs in the past). For BPG, we used the non-default 4:4:4 chroma format following [21]. We also compared our results to JPEG [29] and WebP [13], but they failed to reach our low bit rates and therefore are not shown here. Following [17], and to perform a fair comparison, for each image in the test set, we extracted the sets of matching bpps and MS-SSIM measurements. Since each image has a different rate-distortion curve, we created for each image an interpolated curve and averaged the curves for all test images using a dense bpp grid. We did the same for the baseline model, BPG and JPEG 2000.

We report the results in Figure 5. As can be seen, our method (using side information) outperformed all compared methods. In addition, when comparing the two datasets, *KITTI Stereo* achieved greater improvement than *KITTI General* when using side information. This is aligned with the theory stating that the more correlated X and Y , a more significant improvement can be achieved.

In Figure 6, we visually compare reconstructed images compressed using our approach to the model without side information as well as to JPEG 2000 and BPG. It can be seen that using side information improves the reconstruction - new details that were lost due to the compression are recovered as well as the color that was lost in the quantization process.

Correlation test: The DSC theorem implies that as the correlation between X and Y grows, so does the contribution of Y in compressing X . We have seen this indirectly when analyzing the results of *KITTI Stereo* and *KITTI General*.

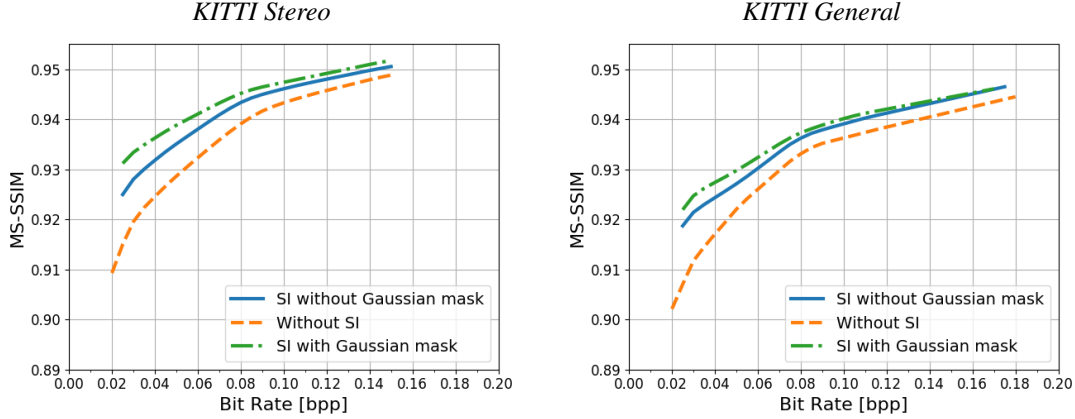


Figure 8. Comparison between models trained with and without a 2D Gaussian mask. It can be seen that the results of *KITTI Stereo* were improved the most, as expected when using the mask.

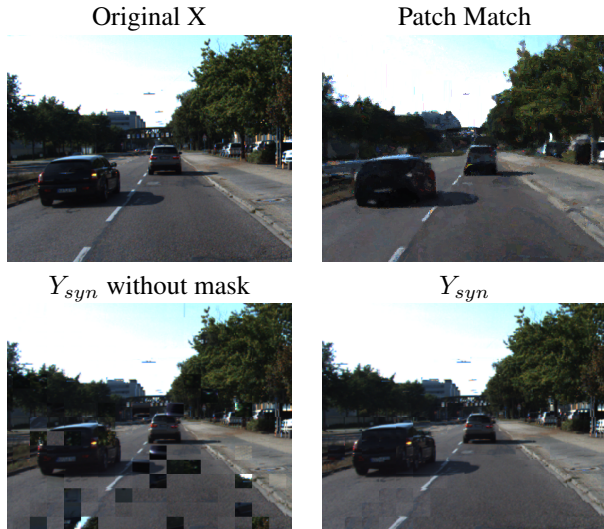


Figure 9. Three different approaches to creating Y_{syn} . Top right: theoretical PathMatch based side information, bottom: the creation of the side information with and without a 2D Gaussian mask. As can be seen, using the 2D Gaussian mask as a prior improved the creation of Y_{syn} .

We now measure this connection directly. Specifically, we examined the relationship between the correlation of (X, Y_{syn}) and the improvement (in percentage) in MS-SSIM, between the model with and model without side-information. For each test image, we calculated the average Pearson correlation between non-overlapping patches of size (20×24) in X and their corresponding patches in Y_{syn} . We then computed the ratio of the MS-SSIM score of the reconstructed image \hat{X} using the model with side-information to that without. We followed this procedure for three tested bpp rates and report the results in Figure 7. As expected, there is a direct link between correlation and

reconstruction improvement. A higher correlation leads to better reconstruction results.

While all curves show positive relation, each curve (i.e., each different rate) has a different exponential growth, which means that providing Y_{syn} with a similar Pearson correlation score to different bit rates models will result in a more significant improvement for the lower bit rates. We argue that this behavior relates to the fact that Pearson correlation is biased towards structures, i.e., the higher frequencies, which are hurt the most at lower bit rates. By using this metric to create Y_{syn} , we provide the structural information that is more beneficial in the lower bit rates.

4.3. Ablation study

Guided Search: A major challenge in our technique is the matching step in which we attempt to find the correct patch in Y for every patch in X . The results so far are based on pure visual search. However, in some cases, we might have additional information that can be used. In particular, we assume that given a patch in X , its corresponding patch in Y should be roughly in the same location in the image plane. We enforce this assumption using a 2D Gaussian mask that helps weight patch similarity in the SI-Finder block. The mean of the mask is taken to be the position of the patch in the image plane, and the variance of the mask is roughly half image size in both axis. This encourages the SI-Finder block to pick patches in Y from roughly the same location, in the image plane, as the patch in X .

To verify the impact of the mask on our system, we trained the full model using the SI-Finder block with and without the use of the mask. See Figure 8. The use of the mask improved results for most bpp (except for a single point). In Figure 9, we present an example of creating Y_{syn} with and without a 2D Gaussian mask. As can be seen, the mask helps the algorithm pick better patches,



Figure 10. Reconstruction examples from *KITTI Stereo* compressed using very low bpp with and without the use of side information. Complete objects, fine details and color are restored.

especially in smooth regions where the Pearson correlation score fails. For comparison, we tested PatchMatch [5] to recover side information by comparing X_{dec} to Y_{dec} and taking the patches from Y . This scenario is not practical because PatchMatch does not run in the network, but it serves as a possible upper bound. As can be seen, the recovered side information using PatchMatch, in this case, looks much better. But upon close inspection, it can be seen that the high-frequency details are distorted. We tested using PatchMatch based side information and got results worst than the once reported here. Nevertheless, we leave the integration of PatchMatch into our network as a possible future research direction. In Figure 10 we share additional reconstruction examples trained using the Gaussian mask and compressed to very low bit rates (that BPG failed to reach) on *KITTI Stereo*.

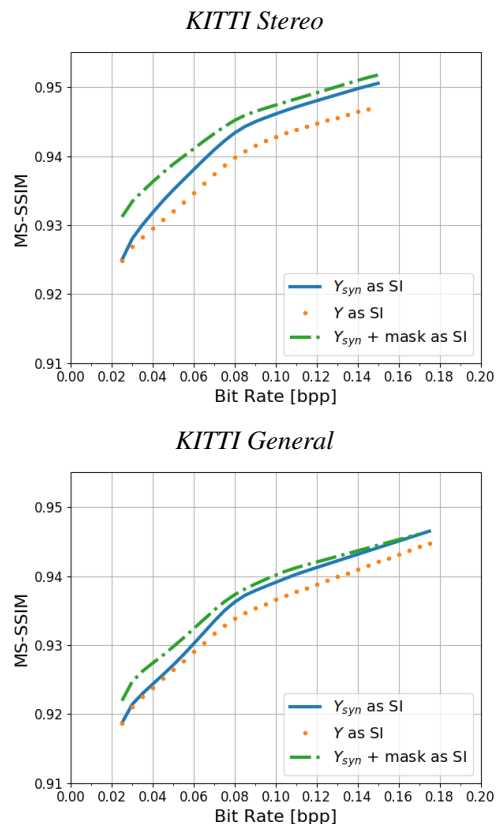


Figure 11. Results using original Y image as side information compared to Y_{syn} (with and without the Gaussian mask). It can be seen that using Y_{syn} improves performance.

Y instead of Y_{syn} : To show the benefit of Y_{syn} , we trained new models (for all the bit rates) using the image Y 'as is'. That is, we concatenated the image Y directly with X_{dec} and skipped the entire block of the SI-Finder. We compared the result to the models trained with Y_{syn} and $Y_{syn} + \text{Gaussian mask}$. As can be seen in Figure 11, using Y as side information gives results that are inferior to the models trained with Y_{syn} .

5. Conclusions

We proposed a novel Deep Image Compression neural network with decoder-only side information. The proposed algorithm relies on the fact that it is possible to improve the compression of an image at the encoder, given that there is a correlated image available only at the decoder. This scenario is quite common in practice, and we considered two such cases. The first is the case of a camera array, and the second is the case of uploading an image to the cloud, where similar images from the same location are already stored. Experiments that were designed to mimic these scenarios show the advantages of our approach.

References

- [1] Anne Aaron, Shantanu Rane, Rui Zhang, and Bernd Girod. Wyner-ziv coding for video: applications to compression and error resilience. *Data Compression Conference*, pages 93–102, 2003. 3
- [2] Anne Aaron, Rui Zhang, and Bernd Girod. Wyner-ziv coding of motion video. *Asilomar Conference on Signals, Systems and Computers*, 1:240–244, 2002. 3
- [3] Eirikur Agustsson, Michael Tschannen, Fabian Mentzer, and Radu Timofteu and Luc Van Gool. Generative adversarial networks for extreme learned image compression. *International Conference on Computer Vision*, 2019. 3
- [4] Johannes Ballé, Valero Laparra, and Eero P. Simoncelli. End-to-end optimized image compression. *International Conference on Learning Representations*, 2017. 2
- [5] Connelly Barnes, Eli Shechtman, Adam Finkelstein, and Dan B. Goldman. PatchMatch: a randomized correspondence algorithm for structural image editing. *ACM Transactions on Graphics*, 28(3), 2009. 8
- [6] Fabrice Bellard. BPG image format. <https://bellard.org/bpg/>, 2014. 6
- [7] Sylvie Chambon and Alain Crouzil. Colour correlation-based matching. *International Journal of Robotics & Automation*, 20, 2005. 6
- [8] David Chen, David Varodayan, Markus Flierl, and Bernd Girod. Wyner-ziv coding of multiview images with unsupervised learning of disparity and gray code. *IEEE International Conference on Image Processing*, pages 1112–1115, 2008. 3
- [9] Qifeng Chen, Jia Xu, and Vladlen Koltun. Fast image processing with fully-convolutional networks. *International Conference on Computer Vision*, pages 2516–2525, 2017. 4
- [10] Thomas M. Cover. A proof of the data compression theorem of slepian and wolf for ergodic sources. *IEEE Transactions on Information Theory*, 21(2):226–228, 1975. 3
- [11] Andreas Geiger, Philip Lenz, and Raquel Urtasun. Are we ready for autonomous driving? the kitti vision benchmark suite. *Computer Vision and Pattern Recognition*, 2012. 6
- [12] Bernd Girod, Anne Margot Aaron, Shantanu Rane, and David Rebollo-Moneddero. Distributed video coding. *Proceedings of the IEEE*, 93(1):71–83, 2005. 3
- [13] Google. WebP image format. <https://developers.google.com/speed/webp/>. 6
- [14] Diederik P. Kingma and Jimmy Ba. Adam: A method for stochastic optimization. *arXiv*, abs1412.6980, 2014. 6
- [15] Didier Le Gall. MPEG: a video compression standard for multimedia applications. *Communications of the ACM*, 34(4):46–58, 1991. 3
- [16] Guo Lu, Wanli Ouyang, Dong Xu, Xiaoyun Zhang, Zhiyong Gao, and Ming-Ting Sun. Deep kalman filtering network for video compression artifact reduction. *European Conference on Computer Vision*, pages 591–608, 2018. 3
- [17] Fabian Mentzer, Eirikur Agustsson, Michael Tschannen, Radu Timofte, and Luc Van Gool. Conditional probability models for deep image compression. *Computer Vision and Pattern Recognition*, pages 4394–4402, 2018. 2, 4, 6
- [18] Moritz Menze, Christian Heipke, and Andreas Geiger. Joint 3D estimation of vehicles and scene flow. *ISPRS-Image Sequence Analysis*, 2015. 6
- [19] Moritz Menze, Christian Heipke, and Andreas Geiger. Object scene flow. *ISPRS - Photogrammetry and Remote Sensing*, 2018. 6
- [20] S. Sandeep Pradhan and Kannan Ramchandran. Distributed source coding using syndromes (discus): Design and construction. *IEEE Transactions on Information Theory*, 49(3):626–643, 2003. 3
- [21] Oren Rippel and Lubomir Bourdev. Real-time adaptive image compression. *International Conference on Machine Learning*, 70:2922–2930, 2017. 6
- [22] David Slepian and Jack K. Wolf. Noiseless coding of correlated information sources. *IEEE Transactions on Information Theory*, 19(4):471–480, 1973. 3
- [23] David S. Taubman and Michael W. Marcellin. *JPEG 2000: Image Compression Fundamentals, Standards and Practice*. Kluwer Academic Publishers, 2001. 6
- [24] Lucas Theis, Wenzhe Shi, Andrew Cunningham, and Ferenc Huszár. Lossy image compression with compressive autoencoders. *International Conference on Learning Representations*, 2017. 2
- [25] George Toderici, Sean M. O’Malley, Sung Jin Hwang, Damien Vincent, David Minnen, Shumeet Baluja, Michele Covell, and Rahul Sukthankar. Variable rate image compression with recurrent neural networks. *International Conference on Learning Representations*, 2016. 2
- [26] George Toderici, Damien Vincent, Nick Johnston, Sung Jin Hwang, David Minnen, Joel Shor, and Michele Covell. Full resolution image compression with recurrent neural networks. *Computer Vision and Pattern Recognition*, 2017. 2
- [27] Yi-Hsuan Tsai, Ming-Yu Liu, Deqing Sun, Ming-Hsuan Yang, and Jan Kautz. Learning binary residual representations for domain-specific video streaming. *Conference on Artificial Intelligence*, pages 7363–7370, 2018. 3
- [28] David Varodayan, Yao-Chung Lin, Aditya Mavlankar, Markus Flierl, and Bernd Girod. Wyner-ziv coding of stereo images with unsupervised learning of disparity. *Proc. Picture Coding Symp*, pages 1–4, 2007. 3
- [29] Gregory K. Wallace. The JPEG still picture compression standard. *Communications of the ACM*, pages 30–44, 1991. 6
- [30] Z. Wang, E. P. Simoncelli, and A. C. Bovik. Multiscale structural similarity for image quality assessment. *Asilomar Conference on Signals, Systems Computers*, 2:1398–1402, 2003. 6
- [31] Chao-Yuan Wu, Nayan Singhal, and Philipp Krähenbühl. Video compression through image interpolation. *European Conference on Computer Vision*, pages 425–440, 2018. 3
- [32] Aaron D. Wyner and Jacob Ziv. The rate-distortion function for source coding with side information at the decoder. *IEEE Transactions on Information Theory*, 22(1):1–10, 1976. 3
- [33] Zixiang Xiong, Angelos D. Liveri, and Samuel Cheng. Distributed source coding for sensor networks. *IEEE Signal Processing Magazine*, 21(5):80–94, 2004. 2

Supplementary Material - Deep Image Compression using Decoder Side Information

2D Gaussian mask As mentioned in section 4.3, we found it beneficial to add a 2D Gaussian mask as a prior in the process of creating Y_{syn} . In Figure 12 we present an example for a correlation map created for a certain patch of X_{dec} by following our method of patch selection as mentioned in 3.2. Furthermore, we compare correlation maps created with and without the use of a 2D Gaussian mask and show their selected matching patches (i.e., patches that yield maximum correlation) marked in Y image. We can see that the 2D Gaussian mask focuses the attention on the more relevant patches.

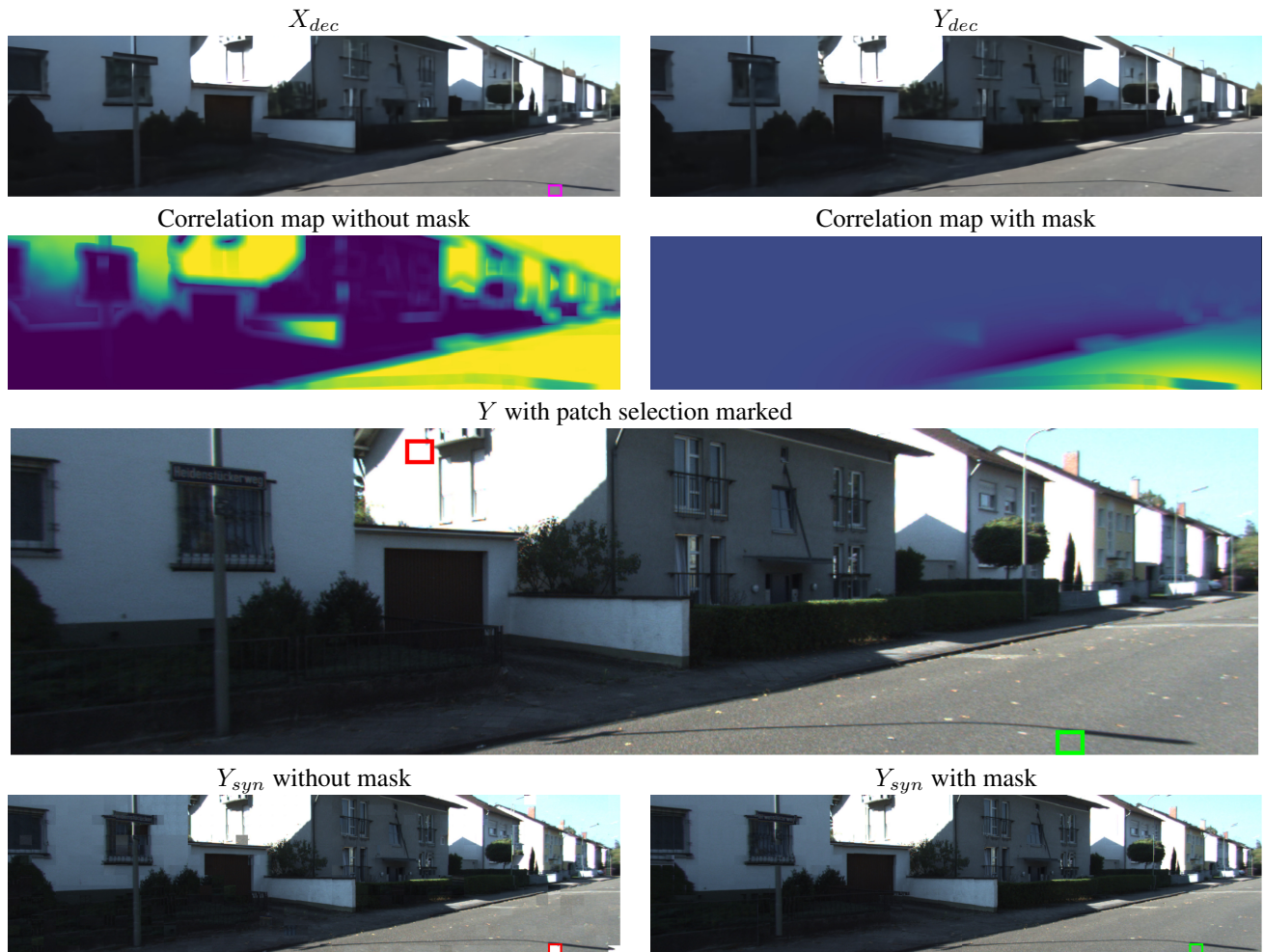


Figure 12. Top to bottom left to right: X_{dec} image with target patch marked in magenta that is compared to all possible patches in Y_{dec} image (top right) and the output, is the correlation map (second row) with and without 2D Gaussian mask (yellow equals high correlation). Third row, Y image with maximum score patches marked. Bottom, Y_{syn} image created with and without the use of the 2D Gaussian mask (the matching patches marked - red patch selected without the mask, green patch selected when using the 2D Gaussian mask).

Reconstruction examples In the next pages, we share additional visual examples for both datasets - *KITTI Stereo* and *KITTI General* compared to the baseline model, BPG, and JPEG 2000. For the other codecs, we chose the reconstruction results with the smallest bpp above ours. When very low bpp is applied, we compare ourselves only with the baseline model since BPG failed to reach these bpps. By observing the results, we can see that JPEG 2000 yields very blurry images, while BPG restores coarse edges well but lacks in textures and fine details. Our model succeeds in restoring edges as well as fine features and textures. When comparing our model with the baseline model, our method does a better job in restoring objects, textures, and colors.

JPEG 2000 0.05225 bpp



BPG 0.05770 bpp



Without SI 0.05241 bpp



With SI 0.05119 bpp

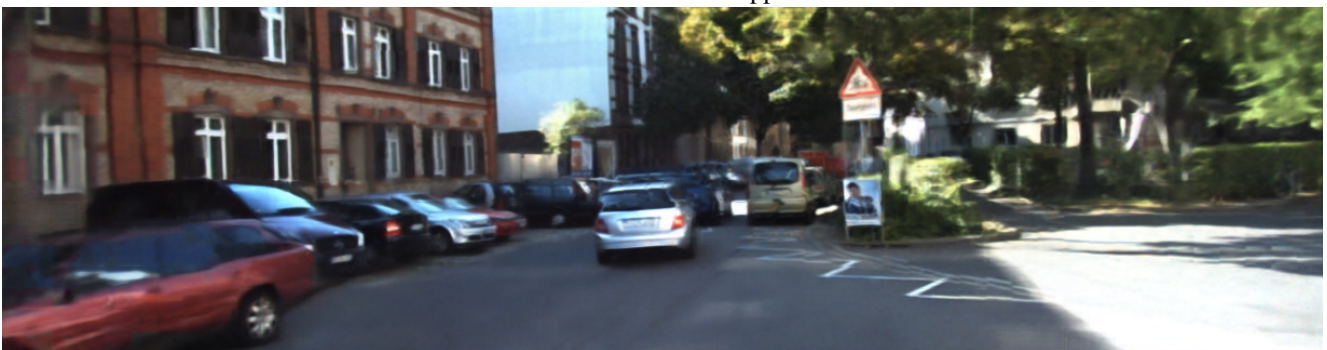


Figure 13. Reconstruction comparison to the baseline model, JPEG 2000 and BPG over *KITTI Stereo*.

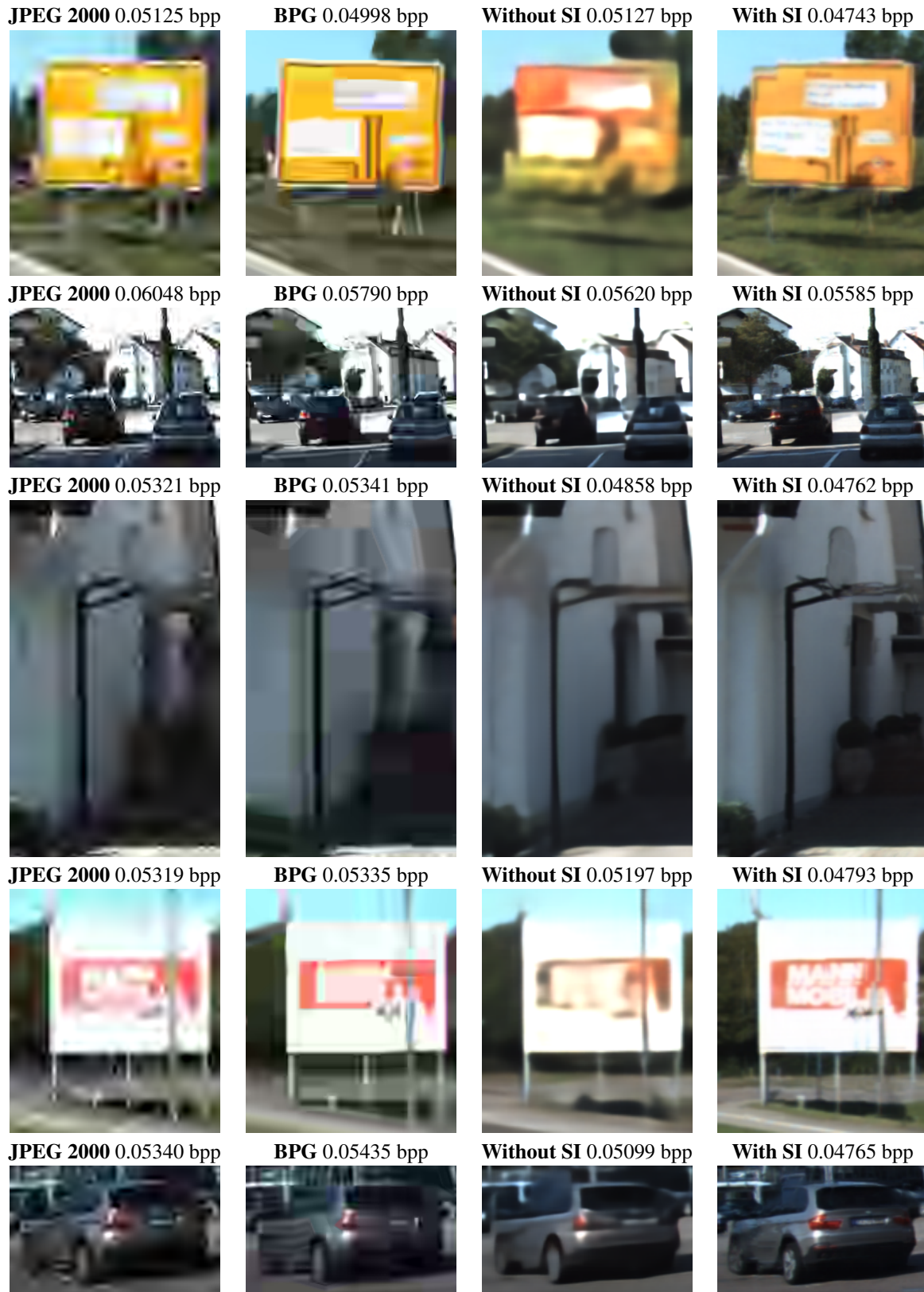


Figure 14. Our suggested method compared with the baseline model, JPEG 2000, and BPG over *KITTI Stereo*.

JPEG 2000 0.06319 bpp



BPG 0.06644 bpp



Without SI 0.06029 bpp



With SI 0.05881 bpp



Figure 15. Reconstruction comparison to the baseline model, JPEG 2000 and BPG over *KITTI General*.

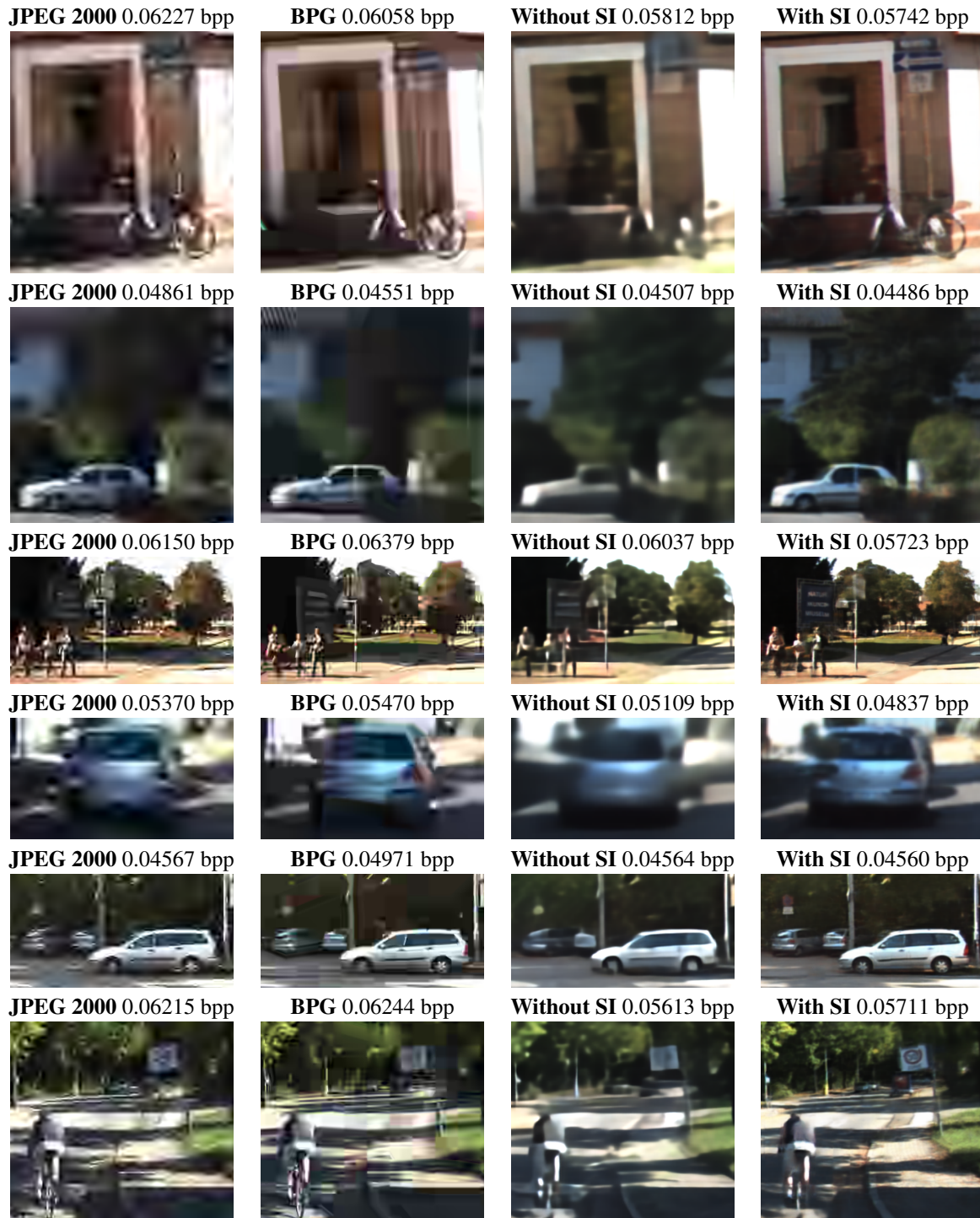
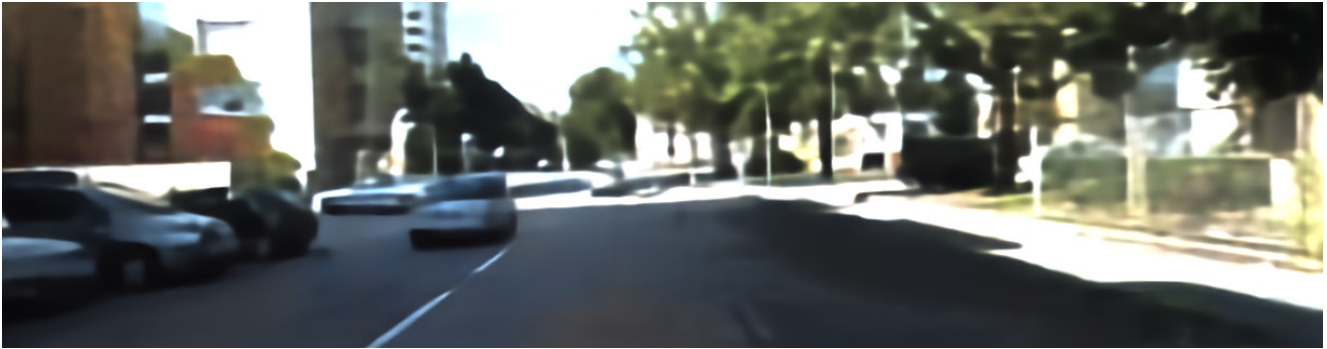


Figure 16. Our suggested method compared with the baseline model, JPEG 2000, and BPG over *KITTI General*.

Without SI 0.03437 bpp



With SI 0.03082 bpp



Without SI 0.02608 bpp

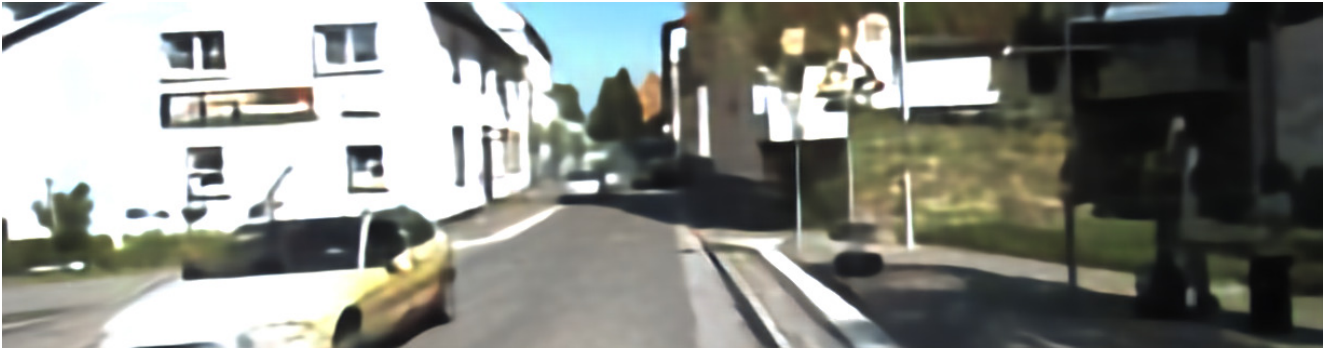


With SI 0.02487 bpp



Figure 17. Reconstruction comparison in low bit rates (that BPG failed to reach) over *KITTI Stereo* with and without side information.

Without SI 0.03931 bpp



With SI 0.03693 bpp



Without SI 0.03105 bpp



With SI 0.02874 bpp



Figure 18. Reconstruction comparison in low bit rates (that BPG failed to reach) over *KITTI General* with and without side information.

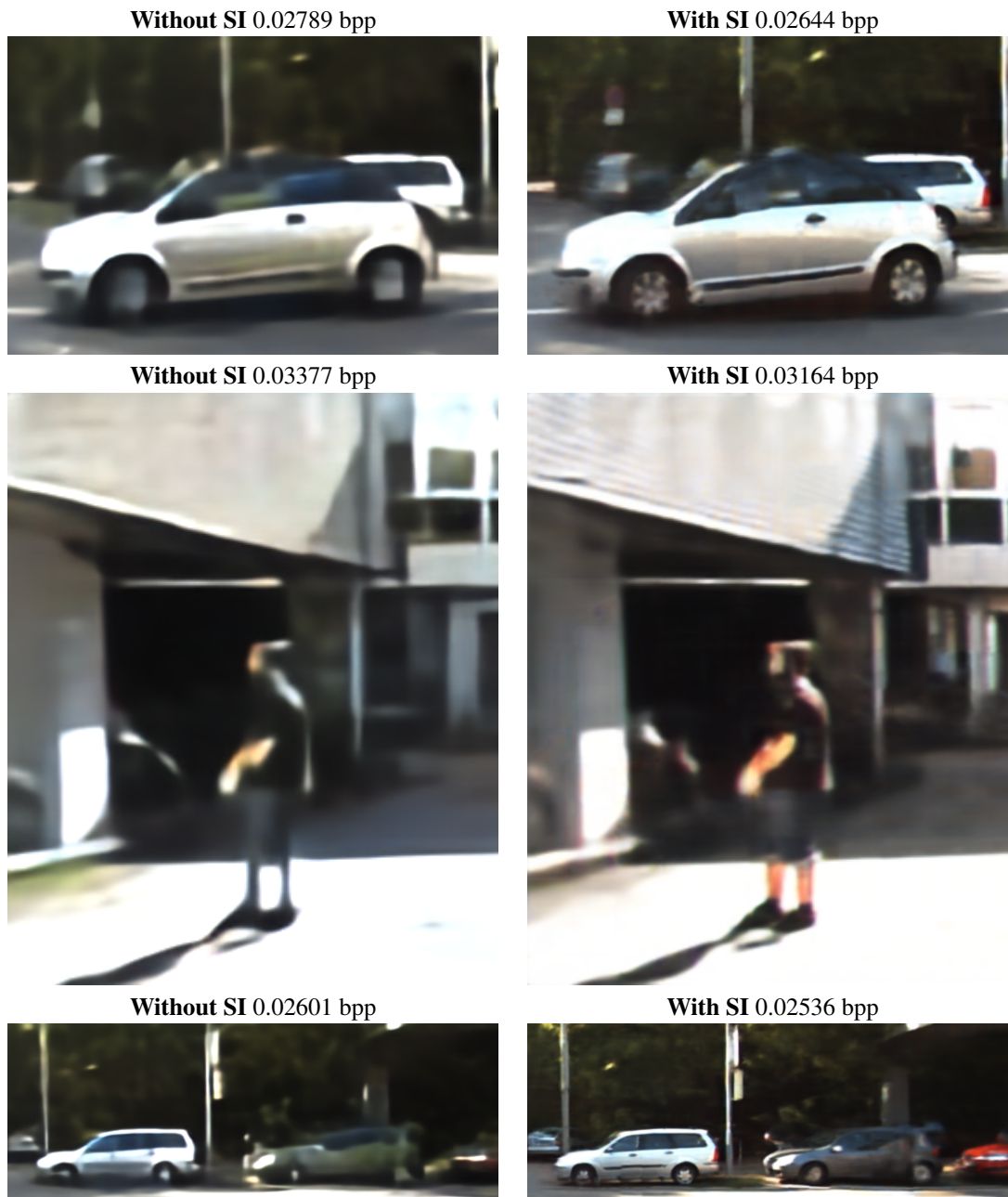


Figure 19. Reconstruction comparison in low bit rates (that BPG failed to reach) over *KITTI General* with and without side information.

Without SI 0.03133 bpp



With SI 0.02981 bpp



Without SI 0.02786 bpp



With SI 0.02760 bpp



Without SI 0.03461 bpp



With SI 0.03228 bpp



Figure 20. Additional reconstruction comparison in low bit rates (that BPG failed to reach) over *KITTI General* with and without side information.